Japanese Journal of Applied Physics 50 (2011) 07HD02 **REGULAR PAPER**
DOI: 10.1143/JJAP.50.07HD02

Design and Fabrication of Fresnel Lens and ZnO Thin-Film Transducer

Min-Chun Pan[1,2], Tuan-Anh Bui[1], Yu-Chuan Nien[1], and Wen-Ching Shih[3]*

[1] *Department of Mechanical Engineering, National Central University, Jhongli, Taoyuan County 32001, Taiwan, R.O.C.*
[2] *Graduate Institute of Biomedical Engineering, National Central University, Jhongli, Taoyuan County 32001, Taiwan, R.O.C.*
[3] *Graduate Institute in Electro-Optical Engineering, Tatung University, Taipei 104, Taiwan, R.O.C.*

Received December 13, 2010; revised February 18, 2011; accepted March 1, 2011; published online July 20, 2011

A four-level Fresnel lens and piezoelectric transducer were fabricated as an ejector using focused ultrasonic energy. The influence of the fabrication parameters on the profile of the focusing lens was investigated. Highly *c*-axis (002)-oriented ZnO films were successfully deposited on Pt (annealed)/Ti/SiO_2/Si substrates under reasonable conditions, such as RF power of 178 W, substrate temperature of 380 °C, deposition pressure of 10 mTorr, and Ar:O_2 gas flow ratio of 50%. These conditions were applied and confirmed through investigating the influence of deposition parameters on the properties of ZnO films. © 2011 The Japan Society of Applied Physics

1. Introduction

Ultrasonic ink jet printing technologies have the potential to produce photographic quality prints that satisfy the demands of fine resolution, high speed, and greater reliability for low-cost printers, which are increasing in commercial use. An ultrasonic focusing ejector[1–6] is capable of ejecting small droplets of controlled diameter from a free liquid surface by focusing high-frequency acoustic waves without using a nozzle; therefore, it is desirable in the fabrication of print-heads. The key elements of an ejector include a piezoelectric transducer and an ultrasonic focusing lens. Different types of ultrasonic focusing lens were investigated and fabricated, such as a spherical lens, a reflection wall,[7] a Fresnel lens,[8–10] a self-focusing acoustic-wave liquid ejector,[11] and a new type of lens using an air chamber as an acoustic reflector, which required no tight control of thickness for effective focusing.[12] Among these ultrasonic focusing lenses, Fresnel lenses offer advantages of planar geometry and relative ease of fabrication over other forms of lenses, but the geometry is critical for efficient focusing, and thus tight control of the thickness of lens elements is usually required. The design and fabrication of "binary" acoustic Fresnel lenses, which use multiple-phase levels to approximate the curvature of a spherical focusing field and offer high efficiencies, were carried out.[9]

Piezoelectric transducers have been used to generate ultrasound, which is subsequently focused by an acoustic lens for the purpose of droplet ejection. ZnO is a promising material that has been well studied and widely applied in piezoelectric transducers and sensors such as ultrahigh frequency surface acoustic wave devices[13] and bulk acoustic wave resonators owing to its good piezoelectric properties and high electro–mechanical coupling coefficient. To enhance high-quality ZnO films, various deposition techniques have been employed and developed such as sputtering,[13–15] metal–organic chemical vapor deposition, and pulsed laser deposition. The properties of ZnO films strongly depend on the deposition conditions such as bottom-electrode materials[16–18] and other fabrication parameters including sputter power,[17,18] deposition pressure, substrate temperature,[18,19] and argon and oxygen (Ar:O_2) gas flow rate ratio.[16,18–20]

In this study, the RF magnetron sputtering method, which offers a simple process with low equipment cost, was employed to develop a feasible means to fabricate thick ZnO films. The effects of deposition conditions, especially the postannealing of the bottom-electrode material, on the growth of ZnO films were investigated. The ZnO films were sputtered on various substrates such as Pt/Ti/SiO_2/Si and Pt(annealed)/Ti/SiO_2/Si. The properties of these fabricated ZnO films were measured to confirm their high *c*-axis orientations, for the ZnO films have potential in the application of high-frequency transducers. In addition, four-level Fresnel lenses with operating frequencies of 100 and 200 MHz were designed and fabricated using micro-electro-mechanical systems (MEMS).

2. Experimental Procedure

2.1 Realization of Fresnel lenses

Ultrasonic focusing lenses need high acoustic energy to expel ink droplets. A highly efficient concentration of sound energy is desirable for this purpose. Ideally, the acoustic focusing efficiency approaches 100% for a focusing lens with spherical geometry, but it is difficult to fabricate, especially using MEMS technology. This is also a problem of great concern. Other proposed focusing lenses can be used as an alternative to the conventional spherical lens. The Fresnel lens is mostly preferred over others owing to its planar geometry and relative ease of fabrication but its focusing efficiency is low. Standard acoustic Fresnel lenses have relatively poor efficiencies because the energy couples into various diffraction modes; the typical efficiency is of 40% or less. This requires more than doubling the input power in comparison to spherical lenses. The design and fabrication of "binary" acoustic Fresnel lenses can offer much higher efficiencies.[9] A binary Fresnel lens uses multiple-phase levels to approximate the phase curvature of the spherical focusing field. Regarding the fabrication of a multilevel lens with the photolithographic technique, each exposure process and etching step can create two phase levels. Therefore, 2^N phase levels can be fabricated by using N masks. The formulas of binary Fresnel lenses based on diffraction optics can be evaluated by the radial distances r_q and the step height h corresponding to a given focal length and wavelength. The radial distance r_q is defined as[9]

$$r_q = \left[\left(z_f + q\frac{\lambda_{cm}}{N_{pl}}\right)^2 - z_f^2\right]^{1/2}, \quad (1)$$

where Z_f is the focal length of the lens, N_{pl} is the number of phase levels, and λ_{cm} is the wavelength of the acoustic field

*E-mail address: wcshih@ttu.edu.tw

 © 2011 The Japan Society of Applied Physics

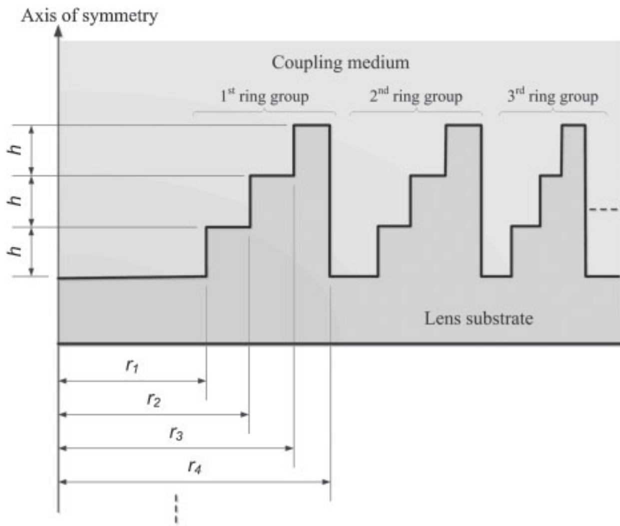

Fig. 1. Basic parameters of designing a four-level Fresnel lens; h is the step height and r_q ($q = 1, 2, 3, \dots$) is the radial distance.

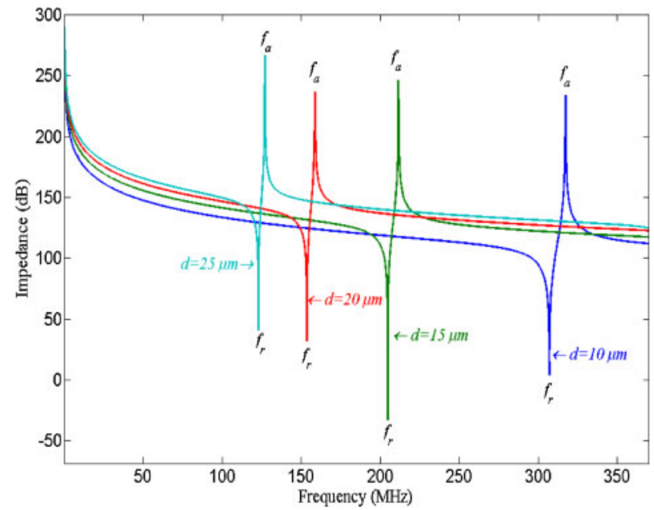

Fig. 2. (Color online) Simulation of the impedance of a piezoelectric transducer under various thicknesses of ZnO film.

in the coupling medium. The step height h between the two phase levels is given as follows:

$$h = \{N_{\mathrm{pl}} f[(C_{\mathrm{cm}})^{-1} - (C_{\mathrm{s}})^{-1}]\}^{-1}, \tag{2}$$

where h is the frequency of ultrasound, and c_{cm} (= 1440 m/s) and c_{s} (= 6375 m/s)[21] are the velocities of sound in the coupling medium and in the lens substrate, respectively. The diffraction efficiency of a multiple phase levels lens is given by

$$\eta = \left[\frac{\sin(\pi/N_{\mathrm{pl}})}{\pi/N_{\mathrm{pl}}}\right]^2. \tag{3}$$

Hence, a four-level Fresnel lens, as shown in Fig. 1, has a theoretical diffraction efficiency of up to 81%.

Substituting these values and other parameters into eqs. (1) and (2), the maximum radial distance and the step height of a 100-MHz focusing lens are obtained as $r_{16} = 244\,\mu\mathrm{m}$ and $h = 4.55\,\mu\mathrm{m}$, respectively. Likewise, the radial distance and step height of a 200-MHz focusing lens, which are $r_{16} = 122\,\mu\mathrm{m}$ and $h = 2.27\,\mu\mathrm{m}$, respectively, may also be obtained.

To complete the fabrication of a four-level Fresnel lens, at least two masks associated with two etching steps were employed, which is fewer processes than are usually required. However, we encountered the disadvantage of nonuniform photoresist coverage because of the high aspect ratio (ratio of the feature height to its width) of the lens. Therefore, currently, a three-mask process associated with three lithographic processes has been considered and applied to address the difficulty. In this study, a four-level Fresnel lens with dimensions as small as 250 μm was successfully fabricated by employing lithography and etching processes. The step height of the lens was too large to coat a photoresist (PR) layer; thus, silicon dioxide (SiO_2) was used as a hard mask in the deep etching process. A 350-nm-thick SiO_2 layer was thermally grown. Through PR coating, exposure, development, and silicon etching, focusing lenses with step heights of 4.55 μm (100 MHz) and 2.27 μm (200 MHz) were shaped. The process using other masks in lithography was repeated until a four-level Fresnel lens was completed.

2.2 Fabrication of piezoelectric transducer

The representation of input impedance in a piezoelectric film/substrate structure has been reported by Lakin *et al.*[22] In this study, we simplified the calculation. The electrical input impedance for a simple one-dimensional resonator having only piezoelectric and perfect electrodes (thickness ~0, an ideal loss-less) can thus be expressed as

$$Z_{\mathrm{in}} = \frac{V}{I} = \frac{1}{j\omega C_0}\left[1 - k_{\mathrm{e}}^2 \frac{\tan(kd/2)}{kd/2}\right], \tag{4}$$

where

$$C_0 = \frac{\varepsilon^{\mathrm{S}} A}{d}, \quad k_{\mathrm{e}}^2 = \frac{e^2}{c^{\mathrm{E}}\varepsilon^{\mathrm{S}}}$$

are the static capacitor and electro–mechanical coupling constant, respectively.[23] k is the acoustic wave number, and d is the thickness of the piezoelectric layer. Equation (4), which is obtained without considering the thickness of the electrodes, can be used to observe the relationship between the piezoelectric film thickness and its corresponding resonant frequency. For efficient acoustic-wave generation, the thickness of the ZnO film is chosen to be an odd number of a half wavelength, which would bring the film into thickness-mode resonance in an air-backed transducer. Consequently, the resonant frequency is inversely proportional to the thickness of the ZnO film.[11] Figure 2 shows the results of a simulation of the impedance of a piezoelectric transducer under various thicknesses of ZnO film. An expression resulting from a simulation of the impedance of the piezoelectric transducer using Matlab under various thicknesses of ZnO films can be written as

$$d \cdot f_{\mathrm{r}} = 3070 \quad (\mu\mathrm{m}\cdot\mathrm{MHz}), \tag{5}$$

where f_{r} is the resonant frequency of the transducer.

With the purpose of investigating the effects of various deposition conditions on the properties of ZnO films, some fabrication trials were performed to find the most appropriate conditions. This study investigated the influence of bottom electrodes on the growth of ZnO films; therefore, other parameters need to be determined in advance. Hence, a

© 2011 The Japan Society of Applied Physics

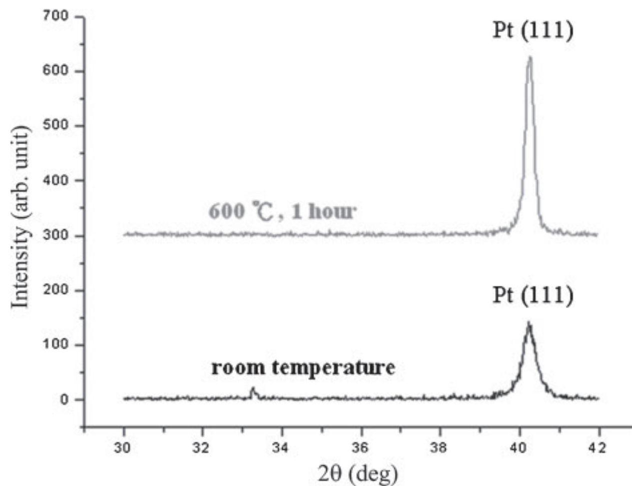

Fig. 3. XRD patterns of annealed and unannealed Pt electrodes.

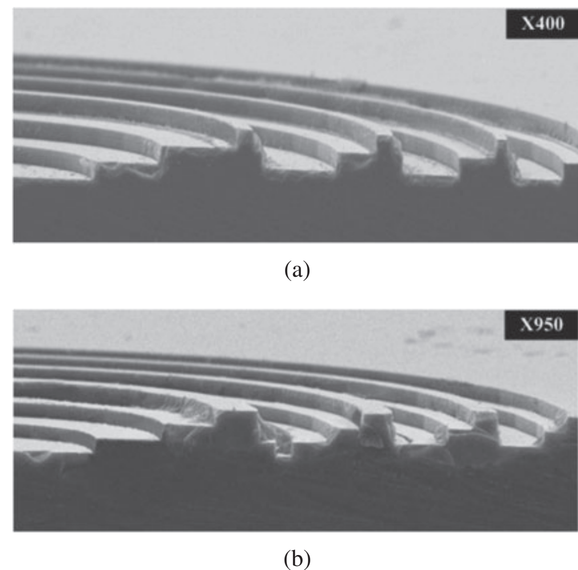

Fig. 4. Oblique view of Fresnel lens from a three-mask process: (a) 100 and (b) 200 MHz.

thin layer of SiO_2 was coated on a cleaned silicon wafer, and a Ti film 20 nm thick was subsequently deposited as a buffer layer to improve the adhesion between the substrate and the bottom electrode. Pt was used as the bottom electrode in the fabrication with a thickness of 150 nm. The transducer structure, therefore, is Al (100 nm)/ZnO/Pt (150 nm)/Ti (20 nm)/SiO_2 (150 nm)/Si.

Based on our previous experiments, the most feasible substrate temperature for sputtering ZnO films is 380 °C, which was again confirmed. Here, 1.3 Pa is the deposition pressure fixed while other factors are varied. The gas flow ratio of Ar:O_2 is maintained as 1 : 1, and ZnO films are sputtered under RF powers of 120, 150, and 178 W. The X-ray diffraction (XRD) patterns of these ZnO films show the highest diffraction intensity in the *c*-axis orientation with an RF power of 178 W. High deposition power leads to high energy of particles that impact on the film surface, increase atom intensity, and tend towards fine columnar grain structure;[24,25] this means a preferred ZnO film is obtained. Similarly, various compositions, 20, 40, and 50%, of oxygen in the sputtering gas were also employed. The most appropriate gas flow ratio of 50% for the *c*-axis (002) orientation of ZnO film growth was determined. More O_2 gas reduces the sputter rate because of higher collision frequency between Ar and O atoms.[24] This may cause a reduction of the energy of particles, reduce the adhesion of particles on the film surface, and affect the *c*-axis crystallographic direction.

To consider the growth of ZnO film on Pt and annealed-Pt bottom electrodes, two sets of samples were separately examined. Yoshino has investigated the effect of bottom electrode films on ZnO film orientation.[26] He found that the crystallinity of the bottom electrode strongly influences the crystallinity of the ZnO film. This is mainly caused by lattice fitting between the ZnO *c*-plane and the surface of the bottom electrode. The XRD patterns of Pt layers exhibiting a better (111) oriented Pt electrode were obtained after annealing in air at an annealing pressure of 1 atm at 600 °C for 1 h after increasing the temperature from room temperature in increments of 10 °C/min (shown in Fig. 3). Finally, ZnO films were deposited on Pt(unannealed)/Ti/SiO_2/Si and Pt(annealed)/Ti/SiO_2/Si substrates through RF magnetron sputtering. The deposition conditions for the ZnO thin films are an RF power of 178 W, a substrate temperature of 380 °C, a sputtering gas ratio (Ar/O_2) of 1 under the fixed setting of a total sputter gas pressure of 1.3 Pa, and a distance between the 4-in. target and the substrate of 45 mm. After the confirmation of XRD patterns, Al evaporation and patterning were performed to shape the top electrode of the transducer. The thickness of the ZnO film was measured by a Dektak^{3}ST α-step surface profiler. The XRD pattern of ZnO films was measured with a Siemens D5000 diffractometer. Finally, the transducer performance was tested through impedance analysis using the Agilent 4395A instrument.

3. Results and Discussion

Since our previous effort on fabricating a focusing lens, we have improved its performance using a three-mask process. The α-step measurement showed a better surface profile of the Fresnel lens in comparison with the two-mask process. An oblique view of the fabricated lens is shown in Fig. 4. It is noted that for the 100-MHz lens the fourth phase level of the lens [Fig. 4(a)] disappeared. The reasons for this are as follows: the coated PR layer was not thick enough, and a uniform coverage was not archived owing to a high aspect ratio, which protects the Si wafer surface during the etching process. In addition, due to the loading effect, the last two rings of the 200-MHz lens had only three phase levels, and the lowest level was not etched; a wafer in a smaller open area etches more slowly compared with that in a larger one. The step height of the fabricated lens shows that there is no significant difference between the designed value and the individually fabricated one.

To consider the variation in radial distances of fabricated lenses, the top view images of the Fresnel lens were captured using an in-line SEM (Fig. 5). We assume that "width" means the difference in radius between two adjacent circles of a fabricated lens. Hence, Table I lists the actual and ideal widths of every ring of the focusing lens. Most of the fabrication errors of the lens widths are acceptable. However, there are still several values that are very different

 © 2011 The Japan Society of Applied Physics

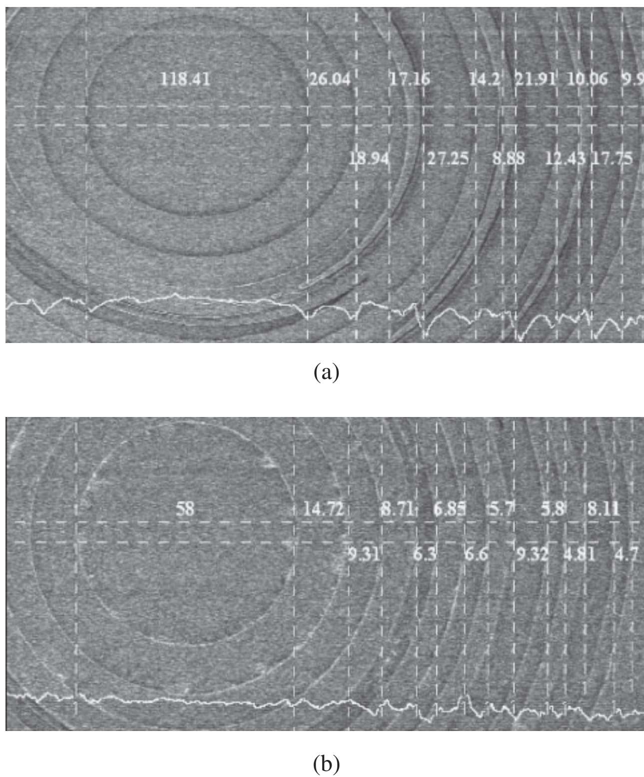

Fig. 5. Top view and adjacent radii of Fresnel lens: (a) 100 and (b) 200 MHz.

Table I. Comparison between the actual and ideal widths of Fresnel lenses.

No	100 MHz lenses			200 MHz lenses		
	Ideal (μm)	Actual (μm)	Error (%)	Ideal (μm)	Actual (μm)	Error (%)
1	118.77	118.41	0.30	59.38	58	2.38
2	24.75	26.04	5.21	12.38	14.72	15.90
3	19.09	18.94	0.79	9.55	9.31	2.58
4	16.19	17.16	5.99	8.09	8.71	7.12
5	14.34	27.25[a]	0.44	7.17	6.36	12.74
6	13.03			6.52	6.85	4.82
7	12.05	14.2	17.84	6.02	6.58	8.51
8	11.27	8.88	21.21	5.64	5.68	0.70
9	10.64	21.91[a]	5.54	5.32	9.32[a]	10.21
10	10.12			5.06		
11	9.67	12.43	28.54	4.83	5.8	16.72
12	9.29	10.06	8.29	4.65	4.81	3.33
13	8.96	17.76[a]	0.85	4.47	8.11[a]	7.84
14	8.65			4.33		
15	8.4	9.9	17.86	4.2	4.7	10.64

a) Two adjacent widths are included.

from the others. The major probable cause of this result is that the values include a measurement error in the adjacent widths due to difficulty in distinguishing their borders. Some levels of the lens are not shaped clearly because of the reasons explained above.

After a two-and-a-half-hour deposition, a ZnO film with a thickness of about 3.7 μm (from α-step measurement) was obtained. The XRD patterns were subsequently measured to

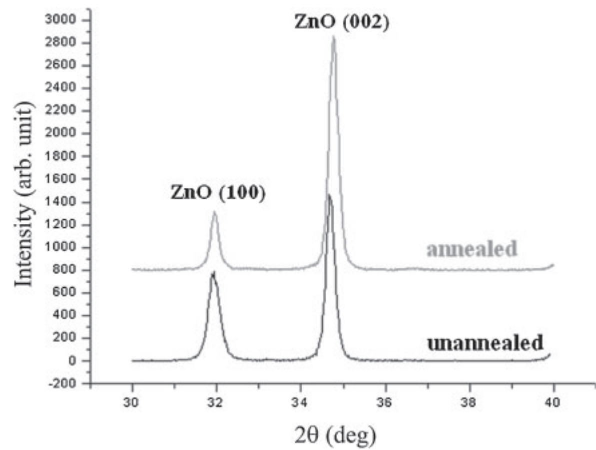

Fig. 6. XRD patterns of ZnO films deposited on Pt electrodes.

Table II. Summary of the results of XRD for ZnO films deposited on (a) annealed and (b) unannealed Pt electrodes under the same deposition conditions.

	X-ray intensity of ZnO(002) peak (I_{002})	FWHM of ZnO(002) peak (deg)	Intensity ratio (I_{002}/I_{100})
(a)	2150	0.20	4.24
(b)	1479	0.24	1.89

determine the diffraction intensity before evaporating Al to create the top electrode in order to complete the piezoelectric transducer. Figure 6 charts the XRD patterns of two ZnO films deposited using various conditions of Pt substrates. The ZnO film deposited on the annealed Pt electrode is characterized by an apparently higher (002) orientation than the Pt substrate without annealing. The (002) orientation of the ZnO film with the unannealed Pt electrode is not much higher than other diffraction intensity peaks [i.e., (100) orientation], so it does not satisfy the requirement of a piezoelectric film for integration into a transducer. However, the desired properties were obtained after ZnO was deposited on a Pt layer annealed at 600 °C for 1 h. The results show that the quality of the ZnO film was improved when deposited on an annealed Pt electrode. We summarize the results of XRD measurements (Fig. 6) for ZnO films deposited on annealed and unannealed Pt electrodes under the same deposition conditions in Table II. From Table II, we can see that ZnO films on annealed Pt electrodes possess better film quality with larger intensity (I_{002}), smaller full width at half maximum intensity (FWHM) of the ZnO(002) plane, and higher intensity ratio (I_{002}/I_{100}). The narrower FWHM of the ZnO film indicates that the crystallinity of the films is better, and there is little misalignment of the lattice planes parallel to the substrate surface. The crystallinity of the ZnO film is affected by the crystallinity and surface morphology of the bottom electrode. These results are similar to those reported by Yoshino.[26] The performance of the piezoelectric transducer was finally analyzed in terms of its impedance characteristics. Figure 7 shows the data for transducer performance measured using an impedance analyzer. The resonant frequency was about 186.5 MHz for the 15.28-μm-thick

© 2011 The Japan Society of Applied Physics

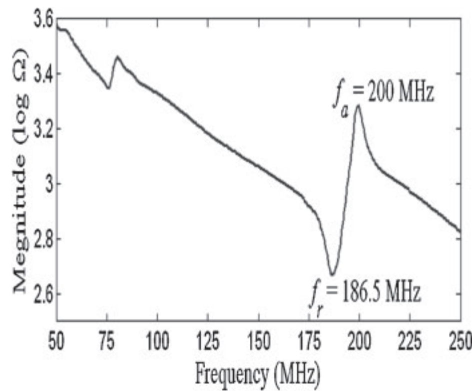

Fig. 7. Transducer performance of the ZnO film with thickness of 15.28 µm measured using an impedance analyzer.

ZnO film. The measured resonant frequency is smaller than the simulated value (200.95 MHz). This is presumably because the mass loading effects caused by the electrodes and the buffer layers on ZnO film leading to the actual resonant frequency are lower than the simulated results. These results are similar to those published by Huang and Kim.[11)]

4. Conclusions

In this paper, the design and fabrication of two main components of an ultrasonic ejector were discussed. As for the performance of fabricated lenses, the required etching depth can be achieved; however, the disadvantages, which can still be improved upon, are that the rings of the 100 MHz lens are only three-level structures, although the last two rings of the 200 MHz lens are four-level ones. The precise profile of a Fresnel lens depends on the uniform thickness of the PR layer in the lithography. The PR thickness is, however, determined by the spin speed and the PR viscosity. Hence, a lower speed is needed to obtain a thicker PR layer. In addition, fabricating a four-level focusing lens using a two-mask process associated with two etching steps is still under investigation, as this process employs one etching step less than the current procedure. A feasible fabrication process for the piezoelectric transducer was proposed and justified by analyzing the influences of the deposition conditions on the properties of ZnO films. Under conditions with an RF power of 178 W, a substrate temperature of 380 °C, a deposition pressure of 10 mTorr, and an Ar:O_2 gas ratio of 50%, ZnO films were successfully deposited on a Pt (annealed)/Ti/SiO_2/Si substrate. These films show a high *c*-axis orientation, which is an essential condition that satisfies the requirements of piezoelectricity for a high-frequency piezoelectric transducer. Impedance analysis shows that the mass loading effects of the electrodes and buffer layers on the ZnO film are significant. We must consider these effects when designing and fabricating a device that works at a specific resonant frequency.

1) S. A. Elrod, B. Hadimioglu, B. T. Khuri-Yakub, E. G. Rawson, E. Richley, C. F. Quate, N. N. Mansour, and T. S. Lundgren: J. Appl. Phys. **65** (1989) 3441.
2) U. Demirci: J. Microelectromech. Syst. **15** (2006) 957.
3) H. Yu, Q. Zou, J. W. Kwon, D. Huang, and E. S. Kim: J. Microelectromech. Syst. **16** (2007) 445.
4) S. C. Tsai, C. H. Cheng, N. Wang, Y. L. Song, C. T. Lee, and C. S. Tsai: IEEE Trans. Ultrason. Ferroelectr. Freq. Control **56** (2009) 1968.
5) J. M. Meacham, M. J. Varady, F. L. Degertekin, and A. G. Fedorov: Phys. Fluids **17** (2005) 100605.
6) H. Fukumoto, J. Aizawa, H. Nakagawa, and H. Narumiya: J. Imaging Sci. Technol. **44** (2000) 398.
7) S. Kameyama, H. Fukumoto, T. Kimura, and S. Wadaka: Proc. IEEE Ultrasonics Symp., 1999, p. 695.
8) B. Hadimioglu, S. A. Elrod, D. L. Steinmetz, M. Lim, J. C. Zesch, B. T. Khuri-Yakub, E. G. Rawson, and C. F. Quate: Proc. IEEE Ultrasonics Symp., 1992, p. 929.
9) B. Hadimioglu, E. G. Rawson, R. Lujan, M. Lim, J. C. Zesch, B. T. Khuri-Yakub, and C. F. Quate: Proc. IEEE Ultrasonics Symp., 1993, p. 579.
10) B. Hadimioglu, S. Elrod, and R. Sprague: Proc. IEEE Ultrasonics Symp., 2001, p. 627.
11) D. Huang and E. S. Kim: J. Microelectromech. Syst. **10** (2001) 442.
12) C. Y. Lee, H. Yu, and E. S. Kim: Proc. 19th IEEE Int. Conf. Micro Electro Mechanical Systems (MEMS 2006), 2006, p. 170.
13) X. Y. Du, Y. Q. Fu, S. C. Tan, J. K. Luo, A. J. Flewitt, S. Maeng, S. H. Kim, Y. J. Choi, D. S. Lee, N. M. Park, J. Park, and W. I. Milne: J. Phys.: Conf. Ser. **76** (2007) 012035.
14) Y. Lin, C. Hong, and H. Chuang: Appl. Surf. Sci. **254** (2008) 3780.
15) J. C. Zesch, B. Hadimioglu, B. T. Khuri-Yakub, M. Lim, R. Lujan, J. Ho, S. Akamine, D. Steinmetz, C. F. Quate, and E. G. Rawson: Proc. IEEE Ultrasonics Symp., 1991, p. 445.
16) R. C. Lin, Y. C. Chen, and K. S. Kao: Appl. Phys. A **89** (2007) 475.
17) Y. H. Hsu, J. Lin, and W. C. Tang: J. Mater. Sci.: Mater. Electron. **19** (2008) 653.
18) S. Chandra, V. Bhatt, and R. Singh: Sadhana **34** (2009) 543.
19) P. M. Martin, M. S. Good, J. W. Johnston, G. J. Posakony, L. J. Bond, and S. L. Crawford: Thin Solid Films **379** (2000) 253.
20) J. Golebiowski: J. Mater. Sci. **34** (1999) 4661.
21) J. Kushibiki, Y. Ohashi, M. Arakawa, T. Tanaka, S. Yoshida, Y. Kourai, and N. Sakagami: Jpn. J. Appl. Phys. **49** (2010) 026602.
22) K. M. Lakin, G. R. Kline, and K. T. McCarron: IEEE Trans. Microwave Theory Tech. **41** (1993) 2139.
23) J. F. Rosenbaum: *Bulk Acoustic Wave Theory and Devices* (Artech House, Norwood, MA, 1988) Chap. 5.
24) S. H. Park, B. C. Seo, G. Yoon, and H. D. Park: J. Vac. Sci. Technol. A **18** (2000) 2432.
25) Y. C. Lin, C. R. Hong, and H. A. Chuang: Appl. Surf. Sci. **254** (2008) 3780.
26) Y. Yoshino: J. Appl. Phys. **105** (2009) 061623.

© 2011 The Japan Society of Applied Physics